

Self-healing ion-permselective conducting polymer coating

Damian Kowalski*, Mikito Ueda, and Toshiaki Ohtsuka

Graduate School of Engineering, Hokkaido University

Kita-13, Nishi-8, Kita-ku, Sapporo, 060-8628, Japan

Fax: (+48) 11-706-65-75

E-mail: kowalski@cat.hokudai.ac.jp

ESI1. Depth distribution of dopants in bi-layered PPy film.

The coating system is composed of two, 2.1 μm thick each, homogeneous layers with the density of 3.4 and 3.6 gcm^{-3} for inner- and outer-layer, respectively.^{1,2} Figure ESI1.1a shows representative surface morphology of the bi-layered PPy coating. The depth profile of the coating system is shown in Fig. ESI1.1b. The glow discharge optical emission spectrum (GD-OES) reveals presence of S, N, C, O, Mo and P elements corresponding to the polymer and doped counter-ions. The spectrum illustrates the bi-layered structure of the polymer and indicates presence of dopants in consecutive layers. The extended outer-layer region and the lower intensity for N and C in the spectrum results from the lower sputtering rate for this layer.³ The XPS spectrum (Fig. ESI1.2) for N1s and S2p indicates highly oxidizing state at the surface. The calculations of the oxidizing state and its relation to the conductivity of PPy have been reported elsewhere.^{2,4} The doping level in the inner-layer is 0.044 and 0.10 for of $\text{PMo}_{12}\text{O}_{40}^{3-}$ and HPO_4^{2-} , respectively.⁴ In addition, the hydrolysis reaction in the inner-layer gives 12 units of MoO_4^{2-} . The hypothetical doping level after full hydrolysis is 0.53 and 0.14 for MoO_4^{2-} and HPO_4^{2-} , respectively, as schematically shown in Fig. ESI1.2c. This simply means that one MoO_4^{2-} ion is doped every 1.9 Py rings and MoO_4^{2-} ions are the major dopants in the inner-layer, if the polymer is exposed to aqueous solution with neutral pH.⁵ It should be noted here that the highest theoretical doping level for PPy arising from reaction stoichiometry is 0.33 negative charges per one Py ring. For as prepared PPy film this value is 0.33 and fits well to the theoretical one. Due to the hydrolysis reaction the number of negative charges offered by MoO_4^{2-} and HPO_4^{2-} is 1.34 per one Py unit and is 4 times as high as possible stoichiometrical number of Py^+ in the polymer backbone chain. According to reaction stoichiometry *ca.* 25% of available anions can be involved in electrostatic interaction with PPy. Approximately 75% anions trapped in the inner-layer film could be involved (i) in nonspecific interaction with the PPy, or ii) in ions pairs with sodium ions. It could be possible that these additional MoO_4^{2-} ions trapped in the inner-layer film are used in the interfacial process at Fe/PPy or are released to the defect zone for self-healing event, whereas amount of whole available MoO_4^{2-} is enough large to balance oxidative state of PPy.

The effect of HPO_4^{2-} ions for self-healing ability is meaningless as predicted by examination “re-passivation” behavior of PPy coating essentially free of HPO_4^{2-} ions (the electropolymerization procedure described in⁴), therefore, is not discussed in details.

The doping level for $\text{CH}_3(\text{CH}_2)_{11}\text{OSO}^-$ (DoS) in the outer-layer is 0.3 evaluated by GD-OES method² and 0.33 by EQCM method in the present study and is close to the theoretical value of PPy oxidation.

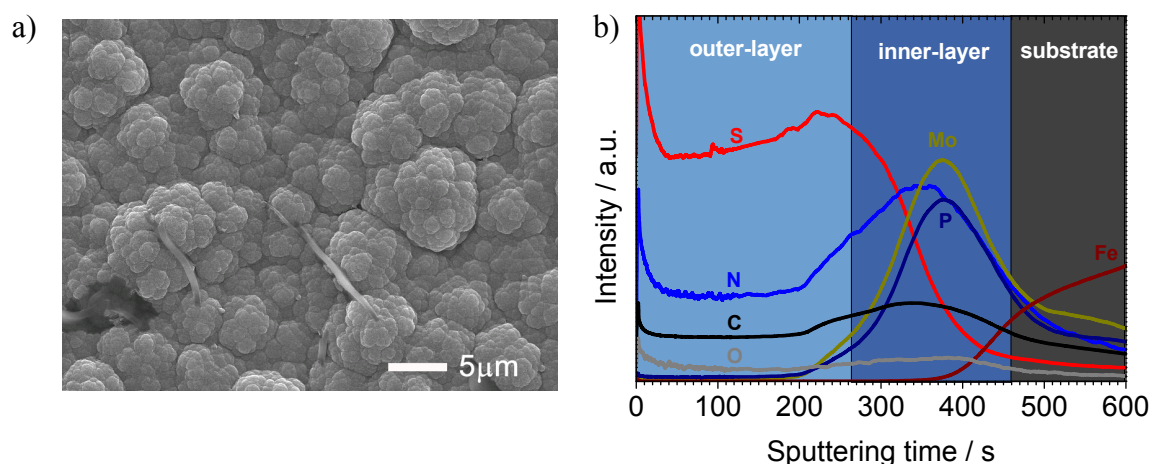


Fig. ESI1.1. a) Surface morphology of the bi-layered PPy film, b) Glow discharge optical emission spectroscopy (GD-OES) depth profile for PPy film electrodeposited on carbon steel with total charge of 2 C cm^{-2} .

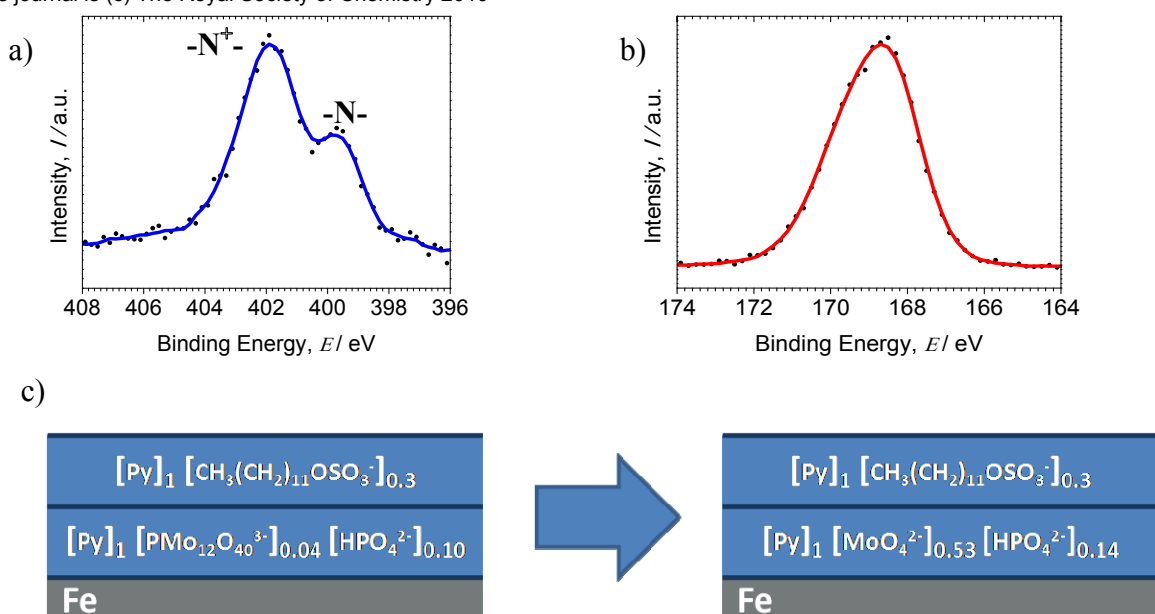


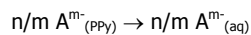
Fig. ESI1.2. a) XPS spectra of N1s, and b) S2p for bi-layered PPY films doped with dodecylsulphate (DoS), c) compositional profile of the bi-layered coating system.

ESI2. Ionic permselectivity of PPY films

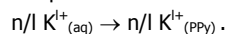
Since corrosion process induce the ionic transport from metal substrate to corrosion solution and opposite polymer can behave like ionic membrane in addition to its electric property. It is likely that the ion-exchange property of ICP may determine the transport of ions which induce the localized corrosion or release of dopants. During the reduction of the PPY matrix,

$$PPy^{n+} + ne^- \rightarrow PPy^0$$

simultaneous release of anion takes place, from PPY to solution,



or uptake of cation from solution to PPY,



For the uptake of cations during the reduction process the native anion dopants must be immobile in the oxidative PPY matrix and thus the cations can move as a charge compensation species. It has been found that ion-exchange property of ICP depend on polymerization conditions,^{6, 7} type and size of counter-ion incorporated into ICP matrix,^{7, 8} its doping level,⁹ ions in the electrolyte solution⁸⁻¹⁰ and pH.¹⁰ In general, PPY films doped with small anions such as Cl^- , NO_3^- , ClO_4^- or SO_4^{2-} , exhibit mainly anion exchange properties due to high mobility of these ions in polymer matrix. The cation exchange behavior was reported for PPY doped with large size organic anions.^{8, 11, 12} Herein, for our permselective layer which should work as ion-gate membrane we investigated four large size organic anions of 2,7-dihydroxynaphthalene-3,6-disulfonate (DHNDS), 1,5-naphthalenedisulfonate (NDS), anthraquinone-1,5-disulfonate (AnqDS), and dodecylsulphate (DoS).

Figure ESI2.1 shows the cyclic voltammetric (CV) response of Au electrode coated by the single PPY- $PMo_{12}O_{40}^{3-}$ film in 3.5 wt.% NaCl solution. The first reduction-oxidation cycle is plotted as a function of scan rate. The mass change on electrode during the first reduction-oxidation scan at a scan rate of 5 mV s^{-1} is also presented.

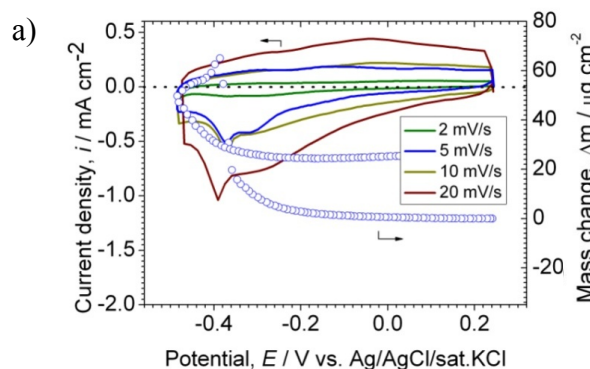


Fig. ESI2.1 Cyclic voltammetric response of Au coated electrode covered by single PPY- $PMo_{12}O_{40}^{3-}$ film in 3.5 wt.% NaCl aqueous solution synthesised with electricity of 100 mC cm^{-2} . First cycle as a function of scan rate. The mass response obtained at 5 mV s^{-1} is plotted by circles.

As seen in figure, two reduction peaks at -0.30 and -0.37 V are observed during the cathodic scan. The first peak is associated with incorporation of cations as a charge compensation species. The corresponding mass change profile shows increase of the mass from -0.24 to -0.37 V. The second cathodic peak revealing larger current is attributed to reduction of PPy and release of small ions like MoO_4^{2-} and/or HPO_4^{2-} . The mass change profile at the first reduction scan shows slight decrease of mass below -0.37 V. The bi-layered film of PPy- $\text{PMo}_{12}\text{O}_{40}^{3-}$ /PPy-DHNDS shows two peaks at -0.34 and -0.36 V in the first cycle, as seen in Fig. ESI2.2a. Similar behavior is observed for PPy film doped with AnqDS in the outer-layer (Fig ESI2.2c).

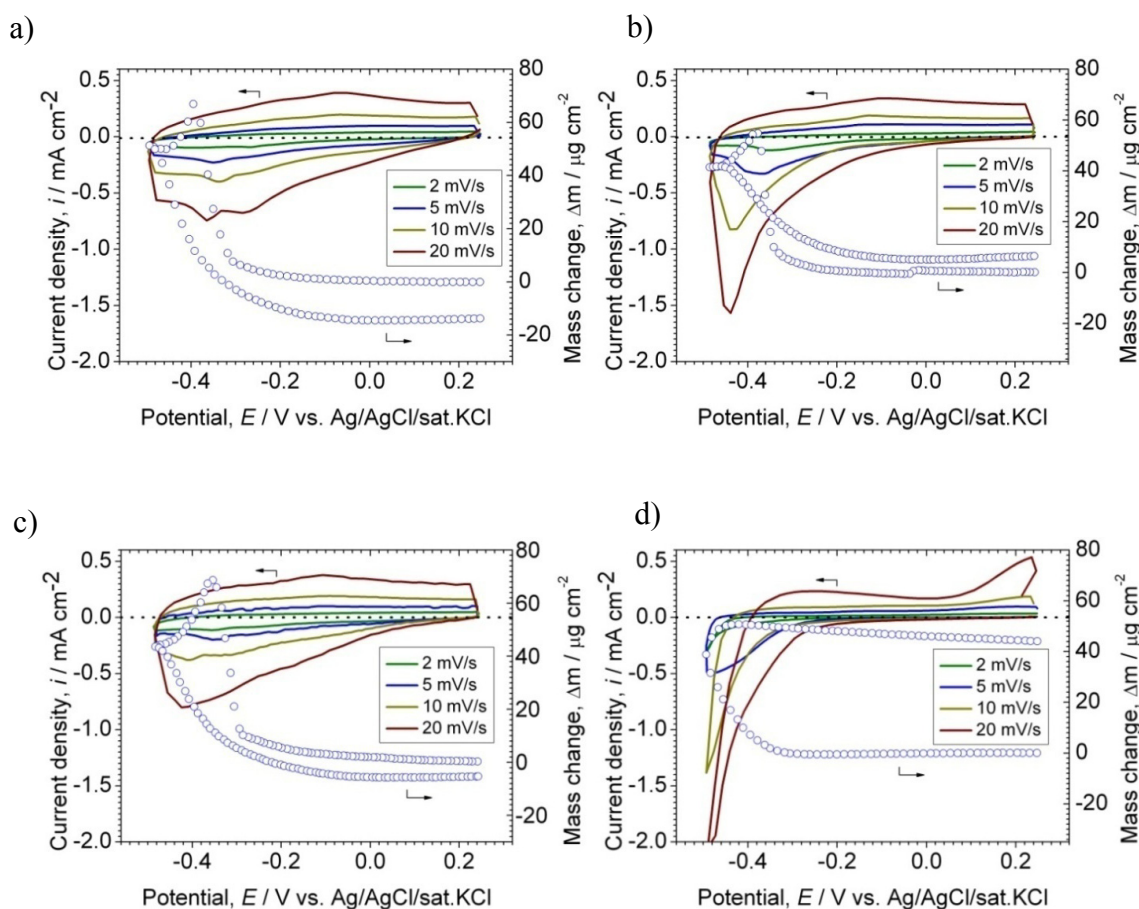


Fig. ESI2.2 Cyclic voltammetric response of Au coated electrode covered by bi-layer film b) PPy- $\text{PMo}_{12}\text{O}_{40}^{3-}$ /PPy-DHNDS, c) PPy- $\text{PMo}_{12}\text{O}_{40}^{3-}$ /PPy-NDS, d) PPy- $\text{PMo}_{12}\text{O}_{40}^{3-}$ /PPy-AnqDS, and e) PPy- $\text{PMo}_{12}\text{O}_{40}^{3-}$ /PPy-DoS in 3.5 wt.% NaCl aqueous solution. Coatings were electrodeposited with the same electricity of 100 mC cm^{-2} . First cycle as a function of scan rate. The mass response obtained at 5 mV s^{-1} is plotted by circles.

Only one cathodic peak is detected at -0.35 V on the voltammogram for PPy- $\text{PMo}_{12}\text{O}_{40}^{3-}$ /PPy-NDS film. The mass for single PPy- $\text{PMo}_{12}\text{O}_{40}^{3-}$ film and for bi-layered films of PPy- $\text{PMo}_{12}\text{O}_{40}^{3-}$ /PPy-DHNDS, PPy- $\text{PMo}_{12}\text{O}_{40}^{3-}$ /PPy-NDS, and PPy- $\text{PMo}_{12}\text{O}_{40}^{3-}$ /PPy-AnqDS increased from +0.25 V to around -0.37 V and decreased from -0.37 V to -0.50 V which indicates cation and anion exchange property at first reduction cycle, respectively.

Different shape of CV was observed for bi-layered PPy- $\text{PMo}_{12}\text{O}_{40}^{3-}$ /PPy-DoS film, as seen in Fig. ESI2.2d. Only one cathodic peak at -0.5 V is seen on voltammogram. This peak is shifted to the more negative values if compared with the PPy film doped with the other organic anions.

Figure 1b shows CV during 17 reduction-oxidation cycles for single PPy- $\text{PMo}_{12}\text{O}_{40}^{3-}$ film. The reduction peaks at -0.30 and -0.37 V decay at the second reduction scan. At the first oxidation scan a peak appears at -0.11 V. This peak is associated with Cl^- ingress to PPy matrix as a charge compensation species. This peak is also observed during the second and following cathodic scans and corresponds to release of Cl^- which were previously inserted at oxidation scans. The peaks associated with the Cl^- incorporation were also detected at the voltammograms obtained for bi-layered films of PPy- $\text{PMo}_{12}\text{O}_{40}^{3-}$ /PPy-DHNDS, PPy- $\text{PMo}_{12}\text{O}_{40}^{3-}$ /PPy-NDS, and PPy- $\text{PMo}_{12}\text{O}_{40}^{3-}$ /PPy-AnqDS (not shown here) which indicate their permselectivity to chlorides.

Fig. 1c. shows 17 reduction-oxidation cycles for bi-layered PPy- $\text{PMo}_{12}\text{O}_{40}^{3-}$ /PPy-DoS film. As compared to the other CVs this film showed response with smaller area under the peak. The peaks associated with the Cl^- incorporation were not detected on the voltammogram.

The mass response from the EQCM electrode coated by single PPy- $\text{PMo}_{12}\text{O}_{40}^{3-}$ film is shown in Fig. 1d. The mass change profile was obtained after 16th reduction-oxidation scan. During the reduction cycle decrease of mass from +0.25 to -0.18 V is observed. This means that during reduction of PPy the anions release from polymer matrix as a charge compensation species. From -0.18 to -0.50 V the mass increases

indicating incorporation of cations from electrolyte to polymer matrix. During oxidation cycle the mass decrease from -0.5 to -0.18 V and increase from -0.18 to +0.25 V indicating release of cations in the first potential region and incorporation of Cl^- in the second one.

The mass change profiles for bi-layered PPy films are shown in Fig. 1e and ESI2.3. The PPy- $\text{PMo}_{12}\text{O}_{40}^{3-}$ /PPy-DHNDS film (Fig. ESI2.3a) shows anion exchange behavior for potential region from +0.25 to -0.05 V and cation exchange behavior from -0.05 to -0.50 V. Indeed, relatively large mass increase is observed for potential region from -0.4 to -0.5 V. The PPy- $\text{PMo}_{12}\text{O}_{40}^{3-}$ /PPy-NDS film exhibits anion exchange property in all potential region, as shown in Fig. ESI2.3b. The mass profile for PPy- $\text{PMo}_{12}\text{O}_{40}^{3-}$ /PPy-AnqDS film (Fig. ESI2.3c) shows anion exchange behavior in potential region from +0.25 to -0.15 V and cation exchange behavior from -0.15 to -0.50 V. The mass exchanged during reduction-oxidation cycle is lower than that for single PPy- $\text{PMo}_{12}\text{O}_{40}^{3-}$. The PPy- $\text{PMo}_{12}\text{O}_{40}^{3-}$ /PPy-DoS film exhibits cation exchange behavior in all potential region, as shown in Fig 1e.

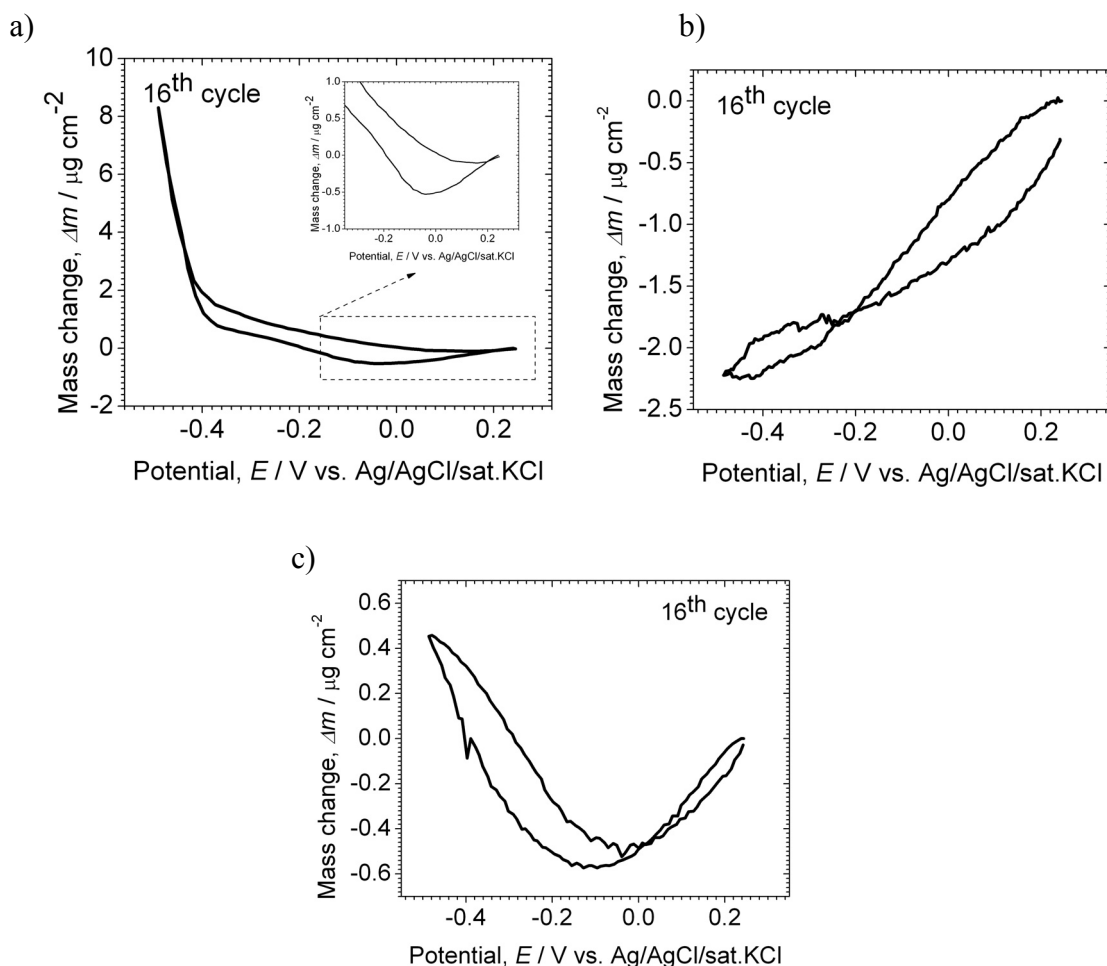


Fig. ESI2.3 The mass change profiles obtained during cycling of Au coated electrode covered by bi-layered film a) PPy- $\text{PMo}_{12}\text{O}_{40}^{3-}$ /PPy-DHNDS, b) PPy- $\text{PMo}_{12}\text{O}_{40}^{3-}$ /PPy-NDS and c) PPy- $\text{PMo}_{12}\text{O}_{40}^{3-}$ /PPy-AnqDS in 3.5 wt.% NaCl aqueous solution. Scan rate was equal to 5 mV s^{-1} .

Interpretation of the first reduction cycle is rather difficult due to complexity of the coating system; however, there is a considerable difference of CV scans between PPy- $\text{PMo}_{12}\text{O}_{40}^{3-}$ /PPy-DoS and other PPy films. Indeed, all investigated coatings showed cation exchange behavior in large potential region, whereas the PPy-DoS layer do not show any permselectivity to anions. The followed scans showed anion or mixed anion and cation exchange property for single PPy- $\text{PMo}_{12}\text{O}_{40}^{3-}$ and bi-layered films of PPy- $\text{PMo}_{12}\text{O}_{40}^{3-}$ /PPy-DHNDS, PPy- $\text{PMo}_{12}\text{O}_{40}^{3-}$ /PPy-NDS, and PPy- $\text{PMo}_{12}\text{O}_{40}^{3-}$ /PPy-AnqDS. The Cl^- ions which induce localized corrosion on steel can penetrate above polymer coatings. In addition, the coating systems show some permselectivity to MoO_4^{2-} ions. The Cl^- ions cannot penetrate PPy- $\text{PMo}_{12}\text{O}_{40}^{3-}$ /PPy-DoS film. Moreover, permselective properties of PPy-DoS layer restrict release of MoO_4^{2-} ions.

ESI3. Self-repair of the coating system

Figure ESI3.1 shows comparison of the open circuit potential (OCP) for bi-layered polymer films of PPy- $\text{PMo}_{12}\text{O}_{40}^{3-}$ /PPy-DoS and PPy- $\text{PMo}_{12}\text{O}_{40}^{3-}$ /PPy-AnqDS in which the artificial defects were formed after 6h immersion in 3.5% NaCl solution. The PPy- $\text{PMo}_{12}\text{O}_{40}^{3-}$ /PPy-AnqDS is not able to self-repair the coating system and restore the passive state of steel (potential oscillations at ca. -0.4 V). Similar OCP curves were

observed for single layered PPy- $\text{PMo}_{12}\text{O}_{40}^{3-}$ and other bi-layered coating systems which are permselective to Cl^- and MoO_4^{2-} ions. In contrast to that the bi-layered PPy permselective to cations (PPy- $\text{PMo}_{12}\text{O}_{40}^{3-}$ /PPy-DoS) possesses ability to restore the passive state of steel (Fig. ESI3.1a).

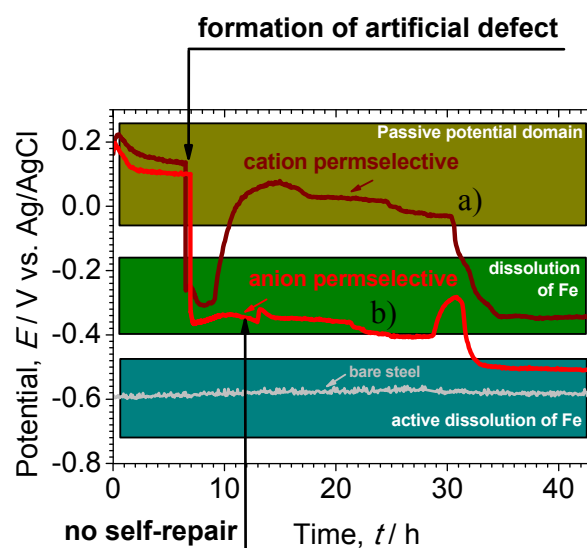


Fig. ESI3.1 Open circuit potential (OCP) for steel coated with bi-layered PPy in which artificial defect was formed after 6h of immersion in 3.5% NaCl solution a) the bi-layered film (PPy- $\text{PMo}_{12}\text{O}_{40}^{3-}$ /PPy-DoS) possessing cation exchange property, b) the bi-layered film (PPy- $\text{PMo}_{12}\text{O}_{40}^{3-}$ /PPy-AnqDS) permselective to Cl^- and MoO_4^{2-} ions.

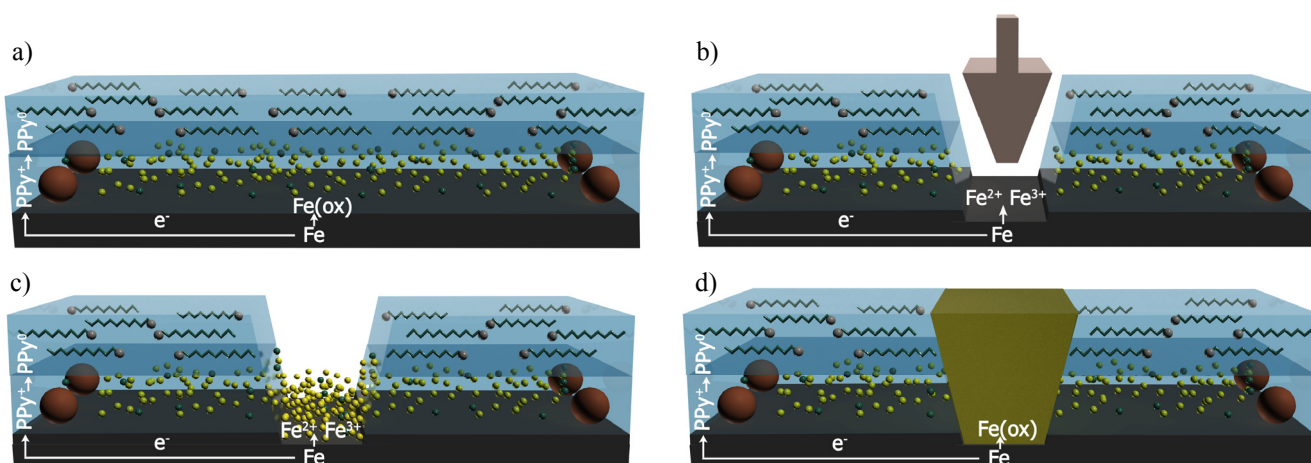


Fig. ESI3.2 The scheme of artificial defect self-repair process in 3.5% NaCl solution. a) The figure illustrates the steel coated with compact bi-layered PPy film during the first 6h of immersion, b) the artificial defect is formed in the coating, c) release of healing ions to the defect zone where they react with dissolved iron, d) self-repair of the coating; formation of insoluble iron molybdate within the defect zone.

Figure ESI3.2 shows scheme of self-repair process in 3.5% NaCl solution. Figure ESI3.2a represents the first 6h of immersion of steel coated with compact bi-layered PPy film. The part of $\text{PMo}_{12}\text{O}_{40}^{3-}$ is decomposed to MoO_4^{2-} and HPO_4^{2-} ions; This stage correspond to the passive potential of steel on OCP graph. In Fig. ESI3.2b the artificial defect is formed in the coating; This stage is associated with the potential drop to -300 mV on OCP graph. Figure ESI3.2c shows release of healing ions to the defect zone where they react with dissolved iron; Oscillations of potential around -300 mV are observed on OCP graph. Figure ESI3.2d represents the formation of iron molybdate within the defect zone blocking dissolution of Fe. The stage is associated with potential increase to the passive domain on OCP graph.

ESI4. Experimental Section

The procedure for electropolymerization of bi-layered PPy on carbon steel has been reported elsewhere.² Electrochemical experiments were carried out using Hokuto Denko HA-501 potentiostat/galvanostat coupled with Advantest R6452A digital multimeter. The EQCM system was

used to monitor mass changes associated with the electropolymerization and reduction-oxidation process. The mass change was measured by change in resonant frequency of Au coated an oscillating AT-cut quartz crystal. EQCM, Maxtec KPS550 sensor was coupled with frequency counter Advantest 5381. The resonance frequency of the quartz crystal was 5 MHz. The theoretical sensitivity for mass detection of the EQCM was $24 \text{ ng Hz}^{-1} \text{ cm}^{-2}$. A three-electrode cell with 250 cm^3 volume was used for EQCM measurements. A Ag/AgCl/sat.KCl and a platinum mesh sheet were used as reference and counter electrodes, respectively. The EQCM measurements were carry out in a Faraday cage. Four types of the bi-layered PPy coatings were prepared on Au coated AT-cut quartz crystal, which consisted of the inner PPy- $\text{PMo}_{12}\text{O}_{40}^{3-}$ layer and the outer PPy layer doped with one of four organic anions of 2,7-dihydroxynaphthalene-3,6-disulfonate (DHNDS), 1,5-naphthalenedisulfonate (NDS), anthraquinone-1,5-disulfonate (AnqDS), and dodecylsulphate (DoS). Before polymerization, all solutions were deoxygenated by nitrogen bubbling for 30 min before use. In the first stage the polymerization was carry out in aqueous solution containing 0.1 M pyrrole (Py) monomer, 0.2 M H_3PO_4 , and 5 mM $\text{H}_3\text{PMo}_{12}\text{O}_{40}$ in which the inner layer of the bi-layered PPy film was formed galvanostatically at a constant current of 1.0 mA cm^{-2} for 50s. The solution was then exchanged with one of the four organic salt solutions: 5 mM 2,7-dihydroxynaphthalene-3,6-disulfonic acid disodium salt (Na_2DHNDS), 5 mM 1,5-naphthalenedisulfonic acid disodium salt (Na_2NDS), 5 mM anthraquinone-1,5-disulfonic acid disodium salt (Na_2AnqDS), and 25 mM sodium dodecylsulphate (NaDoS). In the solution containing 0.1 M Py monomer, the outer layer of the bi-layered PPy film was formed galvanostatically at a constant current of 1.0 mA cm^{-2} . The total electricity for the formation of the bi-layered PPy film was 0.1 C cm^{-2} . For comparison the single layered film of PPy- $\text{PMo}_{12}\text{O}_{40}^{3-}$ was formed with total electricity of 0.1 C cm^{-2} . The cyclic voltammetry was carried out in the same electrochemical cell as polymerization. Cycling tests were done in 3.5 wt.% NaCl aqueous solution. The corrosion tests of the PPy-coated steels were carried out at $25.0 \pm 0.3 \text{ }^\circ\text{C}$ in 3.5 wt.% NaCl solution in which the open circuit potential (OCP) was continuously recorded for 10 days. Depth profile analysis of the anodic oxide films was carried out by GDOES using a Jobin-Yvon 5000 RF instrument in an argon atmosphere of 898 Pa applying RF of 13.56 MHz and power of 40 W. Surfaces of the PPy films were observed by a JEOL JSM-6500F field emission gun scanning electron microscope. Surface analysis was carried out by X-ray photoelectron spectroscopy (XPS) (JEOL JPS-9010TR) using Mg $K\alpha$ ($h\nu = 1253.6 \text{ eV}$). The confocal laser scanning microscopy (CLSM) "Laser-Tech 1LD21D" was used for characterization of the defect created in the coating. A thin gold layer was sputtered on the sample surface before measurements. Laser Raman scattering spectroscopy was used in order to identify the salt formation within the defect. The laser beam was precisely focused inside the defect zone. An Ar gas laser line with 514.5 nm wavelength with 80 mW output power was used for excitation. The Raman scattering light was detected by CCD at the exposure time of 10 s and the integration of 100 times.

- 1 D. Kowalski, M. Ueda and T. Ohtsuka, *Corros Sci*, 2007, **49**, 1635-1644.
- 2 D. Kowalski, M. Ueda and T. Ohtsuka, *Corros Sci*, 2007, **49**, 3442-3452.
- 3 D. Kowalski, Y. Aoki and H. Habazaki, *Angew Chem Int Edit*, 2009, **48**, 7582-7585.
- 4 D. Kowalski, M. Ueda and T. Ohtsuka, *Corros Sci*, 2008, **50**, 286-291.
- 5 T. Ohtsuka, M. Iida and M. Ueda, *J Solid State Electr*, 2006, **10**, 714-720.
- 6 M. A. Vorotyntsev, E. Vieil and J. Heinze, *Electrochim Acta*, 1996, **41**, 1913-1920.
- 7 W. Paik, I. H. Yeo, H. Suh, Y. Kim and E. Song, *Electrochim Acta*, 2000, **45**, 3833-3840.
- 8 C. Weidlich, K. M. Mangold and K. Juttner, *Electrochim Acta*, 2005, **50**, 1547-1552.
- 9 M. Hepel, *Electrochim Acta*, 1996, **41**, 63-76.
- 10 Q. J. Xie, S. Kuwabata and H. Yoneyama, *J Electroanal Chem*, 1997, **420**, 219-225.
- 11 V. Syritski, K. Idla and A. Opik, *Synthetic Met*, 2004, **144**, 235-239.
- 12 M. H. Pyo, J. R. Reynolds, L. F. Warren and H. O. Marcy, *Synthetic Met*, 1994, **68**, 71-77.